THE JOURNAL OF PHYSICAL CHEMISTRY C

Article

Understanding the Spectroscopic Properties and Aggregation Process of a New Emitting Boron Dipyrromethene (BODIPY)

Thanh Truc Vu, Marina Yu Dvorko, Elena Yu Schmidt, Jean-Frédéric Audibert, Pascal Retailleau, Boris A. Trofimov, Robert B. Pansu, Gilles Clavier, and Rachel Meallet-Renault

J. Phys. Chem. C, **Just Accepted Manuscript** • DOI: 10.1021/jp3097555 • Publication Date (Web): 07 Feb 2013

The Journal of Physical Chemistry C is published by the American Chemical Society.
1155 Sixteenth Street N.W., Washington, DC 20036

Understanding the spectroscopic properties and aggregation process of a new emitting Boron Dipyrromethene (BODIPY).

Thanh Truc Vu,[#*] Marina Dvorko,[§] Elena Y. Schmidt,[§] Jean-Frédéric Audibert,[#] P. Retailleau,[†] Boris A. Trofimov,[§] Robert B. Pansu,[#] Gilles Clavier,[#] Rachel Méallet-Renault[#*]

[#] PPSM, ENS Cachan, CNRS UMR8531, 61 av President Wilson, F-94230 Cachan, France

[§] A. E. Favorsky Irkutsk Institute of Chemistry, Siberian Branch of the Russian Academy of Sciences, 1 Favorsky Str., Irkutsk 664033, Russian Federation

[†] Centre de Recherches de Gif sur Yvette, Institut de Chimie des Substances Naturelles, UPR2301-CNRS, 1 avenue de la Terrasse, 91198 Gif sur Yvette cedex France

Supporting Information Placeholder

ABSTRACT: Aggregation of organic dyes has often consequences on their spectroscopic properties in materials. Here, we study a new sterically hindered boron-dipyrromethene (BODIPY), with adamantyl moieties grafted for the first time on the BODIPY core. Its aggregation behaviour was investigated in poly(methyl methacrylate) (PMMA) and on drop-casted films by monitoring absorption, fluorescence emission, relative quantum yield ($\Phi_{Fluo, Rel}$), lifetime and time-resolved anisotropy. Aggregates only appears from 0.067 mol.L^{-1}. A multicomponent analysis demonstrated that the aggregation process can be described by three distinguishable components which correspond to a monomer species (M) and J and H aggregates. The results also indicated a concentration frontier: when the dye concentration increased up to 0.29 mol.L^{-1}, the concentration of M decreased in favour of the aggregates. $\Phi_{Fluo, Rel}$ is yet only divided by five compared to the dye in solution. Above 0.29 mol.L^{-1} an equilibrium between M and the J aggregates is established, showing meanwhile a steady $\Phi_{Fluo, Rel}$. The J aggregates are found to be dimers whereas the aggregation number is varying for the H aggregates. Analysis of fluorescence and anisotropy decays showed that the excitation energy was transferred from M to the J dimers, and very probably trapped by H aggregates.

1. INTRODUCTION

Solid-state fluorescent dyes have attracted much attention because of their potential applications in optoelectronic materials such as organic electroluminescent devices[i] and solid-state dye lasers.[ii] The development of the latest has been important since the mid-1980s to overcome the serious inconveniences of liquid dye lasers linked to toxic solvents and their cumbersome design.[iii] However, in many cases, fluorescent dyes that show intense fluorescence in solution exhibit decreased fluorescence in the solid state as a result of concentration quenching.[iv] Therefore, the number of organic dyes that can show intense fluorescence in the solid state is limited and active research is being conducted to develop such dyes.[v]

BODIPY (4,4-difluoro-4-bora-3a,4a-diaza-*s*-indacene) fluorophores have very good spectroscopic properties: strong visible absorption, narrow fluorescence bands with high quantum yields (Φ_f > 0.7). They are also relatively insensitive to the polarity and pH of their environment and small modifications to their structures enable tuning of their fluorescence emission, from blue[vi] to red[vii] in solution. Their synthesis is relatively straightforward starting from pyrroles.[viii] They can be post modified on various positions.[viiia, ix] Consequently, these dyes are widely used to label proteins[x] and DNA.[xi] Other applications of BODIPY dyes are fluorescent switches,[xii] chemosensors,[xiii] laser dyes,[xiv] and solar cell concentrators.[xv] However, most BODIPY dyes hardly fluoresce in the solid state. This has been attributed to their very small Stokes shift (5–20 nm, in most cases), which increases the probability of energy transfer between the dyes and potentially the trapping of the excitation energy by aggregates. Moreover their high planarity[xvi] favours the π-π stacking, which is well known to lead to a loss of emission efficiency in most cases.[xvii]

Intermolecular coupling in condensed phases can be described with the molecular exciton theory.[xviii] An illustration is given on Scheme 1 for dimer aggregates as an example. This quantum mechanical theory, based on dipole-dipole interaction in the aggregate, predicts a splitting of the excited state of the monomers (initially degenerated at energy E*) into two excited states of energies E(+) and E(-). The selection rules for the electronic transitions, and thus the spectroscopic characteristics of the dimers, depend on the aggregation morphology. In the H-aggregation type, molecular units are aligned parallel (sandwich-like structure, case A) or coplanar displaced with an angle θ >

54.7°: only the transition to the highest excited state is allowed in absorption and the deactivation to the ground state via the lowest excited state tends to be nonradiative.[xix] Formation of H-dimers is thus characterized by hypsochromic shifted absorption bands with respect to the monomer[xx] and no or weak fluorescence emission due to reduced fluorescence rate k_r. In contrast, molecules in J-aggregates are arranged in head-to-tail direction (case B) or coplanar displacements with $\theta < 54.7°$ (case C): only the transition to the lowest excited state is allowed. J-aggregates are characterized by a bathochromic shift of the absorption maximum compared to the monomer and a nearly resonant fluorescence (very small Stokes shift) with narrow band. [xx]

Scheme 1. Exciton splitting of the electronic excited states for different geometric dispositions of the monomer units in a dimer (full line: allowed electronic transition/state; dotted line: forbidden electronic transition/state; ovale-shaped object: monomer unit; double arrow: transition moment).[xviiib, xxi]

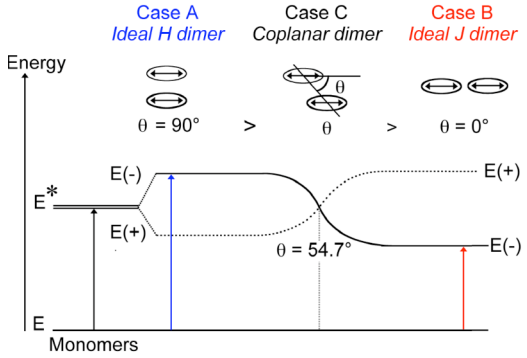

Our strategy to minimize intermolecular interactions and thus molecular aggregation, is to increase the sterical hindrance in the chemical structure: if two dye molecules approach each other, bulky substituents will contribute to prevent the π-systems of the BODIPY core from interacting *i.e* to reduce their tendency to aggregate, and thus to improve the fluorescence quantum yield in solid state. From our previous work, we showed that BODIPY derivatives substituted by one and three mesityl groups are still not bulky enough as we observed the simultaneous formation of both excimers and monomers in the solid state.[xxii] Unfortunately, the formers quenched the fluorescence of the latters. Recently, our group has reported solid-state emissive BODIPY dyes with [2.2]paracyclophanyl moieties introduced at the 3 and 5 positions.[xxiii] These previous results confirmed the necessity to inhibit molecular aggregation and highlighted the effectiveness of sterically bulky substituent(s) in improving the fluorescence quantum yield of BODIPY dyes in solid state. Recently Zhang *et al.* also attempted with success this strategy on the BODIPY platform using 4-tritylphenylethynyl substituents.[xvia]

In this work, we aimed to reduce the π-π stacking by introducing completely saturated bulky substituents such as *adamantyl* group in the 3 and 5 positions of the BODIPY core (compound **AdBdy**, Figure 1). Synthesis of **AdBdy** was possible thanks to our specificity to bring modifications to BODIPY structure not through the aldehyde but the pyrrole.[xxiv] We describe here the aggregation process of **AdBdy** in PMMA films doped with increasing concentrations of the dye. We show from an multicomponent analysis that the aggregation process can be described with a monomer species, a J dimer and H aggregates, the weights of which evolve with the concentration of **AdBdy** in the PMMA matrix. The population ratios of the different species are completely correlated to the spectroscopic features such as the spectra and the fluorescence emission efficiency. Although studies of BODIPY derivatives doped in polymer matrix have been carried out before,[xxv] such a systematic comprehensive study has never been done before, to the best of our knowledge. We show that a high concentration limit exists for aggregation (0.067 mol.L^{-1}). Quite a high fluorescence quantum yield is measured thus **AdBdy** offers great interest for hybrid organic-inorganic materials such as stable organic nano-particles (crystalline or amorphous) grown in sol–gel thin films[xxvi], highly involved in the fabrication of gaz sensors[xxvii].

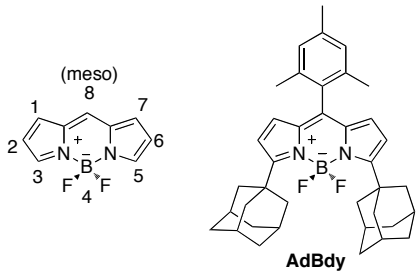

Figure 1. Basic BODIPY framework and its common numbering (left) – Structure of the studied BODIPY derivative (**AdBdy**, right).

2. RESULTS AND DISCUSSION

2.1. Synthesis

AdBdy was synthesized in 70% overall yield, following a standard three-step procedure (Scheme 2) via a condensation of two molecules of pyrroles with mesityl aldehyde followed by oxydation and final complexation with boron trifluoride. The pyrrole was obtained by a modified version of the Trofimov reaction.[xxiv] We choose to introduce a mesityl group in the *meso* (8) position of the BODIPY to impart steric hindrance and ensure high fluorescence quantum yields. Indeed, it has been demonstrated that fluorescence emission is deactivated when an aryl group in *meso* position can rotate freely around the C_{Aryl}–C_{BODIPY} bond.[xxviii] The ortho methyl groups of mesityl impair this motion.

Scheme 2. Synthesis of AdBdy

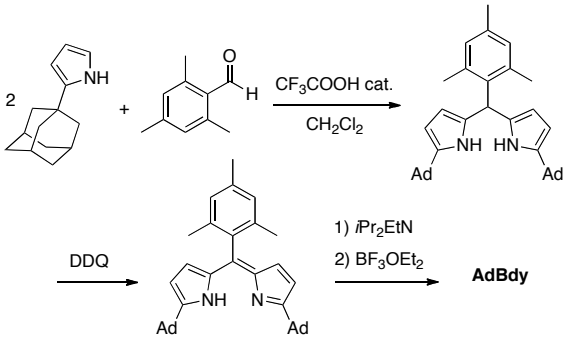

2.2. Quantum Calculations of AdBdy

Quantum chemical calculations have shown that the substitution with adamantyl moieties does not significantly affect either the geometry nor the frontier orbitals of the BODIPY. As a matter of fact, the BODIPY core remains essentially planar and the boron keeps its tetrahedral arrangement despite the sterical hindrance increase due to the adamantyl substituents. The frontier orbitals of **AdBdy** are typical of a BODIPY derivative with an electronic delocalization mainly centered on the core of the fluorophore (Figure S1 in Supporting Information). A small delocalisation can also be observed on the closest alkyl ring of the adamantane for the HOMO, due to the twist between both moieties, imparted by the size of the adamantanes. Energetically, the calculated positions of the orbitals are slightly higher compared to the ones of 8-mesityl-4,4-difluoro-4-bora-3a,4a-diaza-*s*-indacene, as expected from the inductive electron donating effect (+I) effect of alkyl substituents.

2.3. Crystallographic Results.

Suitable crystals for single-crystal X-ray diffraction were obtained by slow evaporation of CH_2Cl_2 solution of **AdBdy** at ambient temperature. As expected, crystal structures show a planar structure for the BODIPY core, a distorted tetrahedral geometry for the boron atom and nearly orthogonal 8-phenyl substituent (dihedral angle of 84.14° for **AdBdy**, Figure 2).

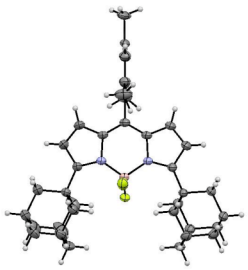

Figure 2. ORTEP view of **AdBdy**.

The distance between the closest overlapping near-parallel π-surfaces (defined by the boradiazaindacene framework, planes A in neighboring unit cells in Figure 3) in **AdBdy** is considerably larger (9.76 Å) than a reference BODIPY dye with no *bulky* subsituent as seen from available crystallographic structure (3.51 Å).[xxix] This is a little bit less than the similar distance (14.3 and 10.1 Å) in BODIPY derivatives with *tert*-butyl substituents on the *meso*-phenyl groups, as reported by Pr. Akkaya's team.[xvii] This clearly indicates that adamantyl groups act as a separator in molecular packing.

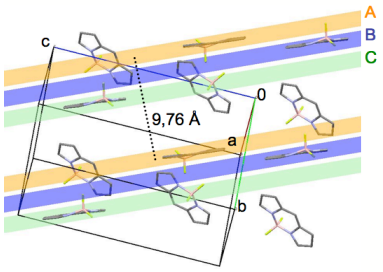

Figure 3. Packing diagram for **AdBdy** (for clarity only BODIPY cores are shown).

2.4. Spectrocopic Properties in Solution.

The spectroscopic features of **AdBdy** in dichloromethane are very similar to those of a standard BODIPY derivative (see figure S2 in SI). The main absorption band at 517 nm is attributed to the 0–0 vibrational band of a strong $S_0 \rightarrow S_1$ transition; the shoulder at its shorter wavelength side is assigned to the 0–1 vibrational band of the same transition.[xxx] This symmetry allowed transition bears a fairly high extinction coefficient (99 500 ± 5% L. mol^{-1} cm^{-1}). A considerably weaker, broad absorption band is found below 450 nm, which is attributed to the $S_0 \rightarrow S_2$ transition. The fluorescence quantum yield is very high (0.79 ± 10%) and the fluorescence lifetime (6.48 ± 0.05 ns) is in the usual range.

The solvent effect on the absorption and fluorescence bands was also studied following the methodology developed by Catalán[xxxi] in which the various types of solute–solvent interactions are described thanks to four independent, yet complementary, solvent parameters: acidity (SA), basicity (SB), dipolarity (SdP) and polarisability (SP). A solvent-dependent physico-chemical property **A** is then formulated as:

$$\mathbf{A} = A_0 + b\mathrm{SA} + c\mathrm{SB} + d\mathrm{SP} + e\mathrm{SdP} \qquad (1)$$

A_0 is the statistical quantity corresponding to the value of the property in the gas phase; and the coefficients *b* to *e* are the regression coefficients describing the sensitivity of property **A** to the different solute–solvent interactions.

The absorption and fluorescence emission spectra of **AdBdy**, recorded in several solvents (see Figure S3 and Table S1 in SI) exhibit very small wavelength shifts (3.5 – 6.5 nm) for the respective maxima. When applying the equation (1) to the absorption ($\bar{\nu}_{abs,\max}$) and fluorescence ($\bar{\nu}_{fluo,\max}$) maxima wavenumbers, we can conclude that **AdBdy** presents a solvatochromism dominated by polarisability (equations (2) and (3)). The calculated values fit quite well to the experimental data (see Figure S4 in SI). The same conclusions were drawn by Catalán on commercial BODIPY dye 567 (PM567) and Böens et al. on BODIPY dye with aza crown ether functionality.[xxxii] This weak solvatochromism was expected since **AdBdy** has no acid base properties on one hand and since the permanent dipole moment varies very little upon excitation, on the

other hand. Such a photophysical property is well suited for our study as the aggregation of **AdBdy** will be investigated in various environments: the possible aggregation effects will be shown directly through the spectroscopic changes since the latest are not to be due to the solvatochromism of the dye.

$$\bar{\nu}_{abs,\max}\ (\text{cm}^{-1}) = (19922 \pm 3) - (768 \pm 2)\text{SP} + (88 \pm 2)\text{SdP} - (63.9 \pm 0.05)\text{SA} - (9 \pm 2)\text{SB} \quad (2)$$

$$\bar{\nu}_{fluo,\max}\ (\text{cm}^{-1}) = (19732 \pm 4) - (1017 \pm 3)\text{SP} + (27 \pm 3)\text{SdP} - (120.5 \pm 0.1)\text{SA} + (64 \pm 2)\text{SB} \quad (3)$$

2.5. Spectrocopic Properties in Polymer Films.

Photophysical studies were carried out on poly(methyl methacrylate) (PMMA) films increasingly doped with **AdBdy** (see Table S2 in SI for composition details). The spectroscopic properties were shown to be homogeneous over each individual film, despite a non negligible variation in the thickness of the BODIPY doped PMMA films (8 – 30 nm): absorption spectra were measured for at least 5 positions on each film and show a variation of only 0.02 for the optical density and 1 nm for the absorption maximum, which is within the measurement accuracy. The absorption and emission spectra of **AdBdy** in PMMA films at concentrations from 0.067 M to 1.2 M are given in Figure 4 and the spectroscopic characteristics are reported in Table 1. Blank samples of PMMA were checked to be non fluorescent and used as reference. Beyond 1.2 M, **AdBdy** precipitates and gives heterogeneous PMMA films (see Figure S5 in SI). The results in PMMA films are compared to data measured in a solution of 40% wt. PMMA in toluene (S_{PMMA}). For concentrations below 0.067 M the same spectroscopic signature as for the monomer in solution can be observed in absorption and with a variation of only 1 to 4 nm for the fluorescence maximum (see Figure S6 in SI), which is within the solvatochromic effect as seen previously. These results let us think that the concentration limit for aggregation can be set at 0.067 M. This first conclusion is greatly promising as this value is much higher that what has been reported for other dyes[xxxiii]. For instance, fluorescein isothiocyanate, incorporated inside colloidal silica spheres, shows a 10 nm red shift in the spectra for a dye content above 0.006 M with the average distance between dye molecules inside the particles being 6.5 nm.[xxxiv]

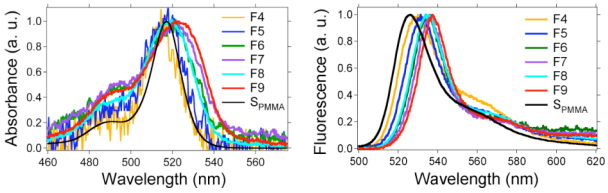

Figure 4. Normalized absorption (left) and fluorescence (right) spectra of **AdBdy** in PMMA at different concentrations.

Table 1. Spectroscopic characteristics of AdBdy in PMMA, at different concentrations. Fluorescence data were recorded with excitation at 488 nm. Empty boxes are due to signals being below the detection limit (F1, F2) .

Film i	C mol.L^{-1}	$\lambda_{abs,\max}$ ± 1 (nm)	$FWHM_{abs}$ ± 27 (cm^{-1})	$\lambda_{fluo,\max}$ ± 1 (nm)	$FWHM_{fluo}$ ± 24 (cm^{-1})
S_{PMMA}	1.1×10^{-5}	517[a]	656[b]	526[c]	824[d]
F1	4.7×10^{-4}	–	–	527	1131
F2	2.3×10^{-2}	–	–	530	941
F3	4.7×10^{-2}	516	810	530	928
F4	6.7×10^{-2}	515	744	529	964
F5	9.4×10^{-2}	518	901	531	813
F6	2.9×10^{-1}	520	1242	535	706
F7	5.9×10^{-1}	522	1232	536	655
F8	8.0×10^{-1}	519	1094	535	755
F9	1.2	523	1343	537	650

[a] ± 0,5 nm [b] ± 38 nm [c] ± 0,25 nm [d] ± 18 cm^{-1}

As the concentration of **AdBdy** is increased up to 1.2 M, the absorption band broadens by roughly a factor of two ($FWHM_{abs}$ going from 656 ± 27 cm^{-1} in S_{PMMA} to 1343 ± 27 cm^{-1} for 1.2 M) and experiences a red shift ($\lambda_{abs,\max}$ going from 517 ± 1 nm in S_{PMMA} to 523 ± 1 for 1.2 M). The broadening occurs both in the lower and higher energy range compared to the absorption band of the monomer: indeed, on one hand, the shoulder at *ca.* 488 nm becomes more intense with the ratio A_{488}/A_{max} increasing from 0.23 ± 0.01 (0.067 M) to 0.31 ± 0.01 (1.2 M) where A_{488} and A_{max} are the absorbance at 488 nm and at the absorption maximum respectively (see Table S3 in SI); on the other hand, although the spectra show no shoulder in the lower energy range, the broadening can be illustrated through the increase of the ratio A_{534}/A_{max} from 0.07 ± 0.05 (0.067 M) to 0.71 ± 0.01 (0.2 M), where A_{534} is the absorbance at 534 nm (see Table S3 in SI). The observed 6 nm shift of $\lambda_{abs,\max}$ can be partially due to solvatochromism as the polarisability in the film can be higher with the increasing concentration of **AdBdy**. However the both-sides broadening can be most probably ascribed to the formation of both H and J aggregates. These last ones are furthermore corroborated by the red shift and the narrowing of the emission band: $\lambda_{fluo,\max}$ shifts from 526 ± 1 nm (S_{PMMA}) to 537 ± 1 nm (1.2 M) and $FWHM_{fluo}$ decreases from 824 ± 18 cm^{-1} to 650 ± 24 cm^{-1}.

Similar spectroscopic changes induced by aggregation were observed in drop-casted films of **AdBdy** insofar as the absorption spectra also showed a band broadening with the $FWHM_{abs}$ increasing up to 2207 ± 27 cm^{-1} and a red shift up to 524 nm for the maximum, in comparison with S_{PMMA} (see Figure S7, left in SI). The fluorescence maximum also displays a red shift up to 540 nm in drop-casted films (see Figure S7, right in SI).

Strictly, we cannot exclude the possibility that part of the red shift in the fluorescence is caused by the inner filter effect: fluorescence on the blue side of the emission spectrum can be suppressed by reabsorption due to

overlap with the absorption spectrum. However the fluorescence spectra of dye doped PMMA films have been corrected of this effect, taking into account the absorption of each sample (see Experimental Section). Besides the absorption spectra show almost the same trends, ruling very likely the inner filter effect out. It was also verified that fluorescence spectra did not depend appreciably on the excitation wavelength as the spectra show no significant difference for excitations at 343, 470 and 488 nm.

In order to have a deeper understanding of the aggregation process in terms of spectroscopic features of the formed aggregates and their relative growth with the increase of the dye doping percentage, a quantitative spectral analysis of multicomponents was carried out on the absorption spectra of both doped PMMA (**F4→F9**) and drop-casted films of **AdBdy** (see Figure S8 in SI). A total of 33 spectra were considered in order to integrate as much information as possible on the aggregation process. Absorption spectra of **AdBdy** in PMMA films with concentrations above 1.2 M were included as they also contained information about the aggregation process (see Figure S9 in SI). Absorption spectra corresponding to concentrations below 0.067 M were not taken into account because of their low signal to noise ratio. This approach was successfully used by M. Kubista to determine the absorption spectra of the four protolytic forms of fluorescein and the corresponding protolytic constants.[xxxv] The analysis of multicomponents was executed by Igor software (Wavemetrics Oregon). Only the four most significant projection vectors $\{\mathbf{PV_{i=1,2,3,4}}\}$ were kept as their weights contain 99.92 % of the starting information, against 99.94 % when taking into account the fifth projection vector (see Figures S10, S11 and Table S4 in SI for more details).

Four projection spectra $\{\mathbf{PS_{i=1,2,3,4}}\}$ (Figure 5, left) were then calculated by linear combinations of the projection vectors, which are indeed mathematical solutions with no photochemical reality (see Equations S1–S4 in SI). This operation has nonetheless some shortcomings. Firstly, the projection spectra are not orthogonal, yet their non colinearity can be easily checked. Secondly, the set of projection spectra is not unique in that there is an infinity of potential linear combinations of $\{\mathbf{PV_{i=1,2,3,4}}\}$ leading to an infinity of basis. In our case, the projection spectra were calculated so they present clear spectroscopic features in terms of absorption bands, with the narrowest FWHM and well defined vibronic structures as far as possible. The projection spectra $\mathbf{PS_4}$ clearly shows a linear dependency on $\mathbf{PS_2}$ and $\mathbf{PS_3}$ (see Figure S12 in SI),, implying only 3 projections spectra can describe the system. Compared to $\mathbf{PS_2}$ and $\mathbf{PS_3}$, $\mathbf{PS_4}$ presents two well-defined spectroscopic features : a blue band and a red one.

Then we deliberately split the projection spectrum $\mathbf{PS_4}$ into two different spectra, named $\mathbf{PS_J}$ (red band) and $\mathbf{PS_H}$ (blue band) in the following discussions (see Figure 5, right). We ended up building a new basis with $\mathbf{PS_1}$ (renamed as $\mathbf{PS_M}$, for convenience as explained below), $\mathbf{PS_J}$ and $\mathbf{PS_H}$. Although this operation is partly arbitrary, the $\{\mathbf{PS_{i=M,\ J,\ H}}\}$ basis gives a better reconstitution of the experimental data, with a smaller residual sum of squares[xxxvi], compared to the $\{\mathbf{PS_{i=1,2,3,4}}\}$ basis, which validates *a posteriori* our approach (see SI for further details).

In mathematical terms, $\{\mathbf{PS_{i=M,\ J,\ H}}\}$ can be considered as a basis so that every element of the vector space can be expressed uniquely as a finite linear combination of basis vectors. From a photophysical point of view, the vector space includes all the aggregation states of **AdBdy** in amorphous condensed phases such as in PMMA or drop-casted films whereas basis vectors correspond to the specific molecular structures likely to be formed in condensed phases. An absorption spectra of **AdBdy** in any amorphous condensed phase ($\mathbf{AS_{exp}}$) can theoretically be described by the set $\{\mathbf{PS_{i=M,\ J,\ H}}\}$ as depicted in equation (4), where $\mathbf{AS_{calc}}$ is the reconstructed absorption spectrum. The contribution of each $\mathbf{PS_i}$ is given by the coefficient $\mathbf{c_i}$. If the component $\mathbf{PS_i}$ corresponds to the specific structure $\mathbf{S_i}$, $\mathbf{c_i}$ is proportional to the concentration of $\mathbf{S_i}$ in the PMMA film and $w_i = c_i/\sum c_i$ to its weight. This correspondence is indeed possible since the absorption spectra initially considered in the analysis of multicomponents were not normalized.

$$\mathbf{AS_{calc}} = c_M\,\mathbf{PS_M} + c_J\,\mathbf{PS_J} + c_H\,\mathbf{PS_H} \qquad (4)$$

The reconstructed absorption spectra $\mathbf{AS_{calc}}$ (equation 4) fit well to the experimental data (Figure 6a and Figure S13 in SI). This check out operation was run by an Igor program. The χ^2 statistics is not relevant to evaluate the goodness of fit here as the noise variance can't be determined since the projection spectra were not *fully* obtained from experimental data. For the three samples displaying the most important discrepancy (considered as corresponding to the highest standard deviation of non weighted residuals, see Figure S13 in SI), the reconstructed absorption spectra still visually fit satisfactorily the experimental data (see Figure 6b). To the best of our knowledge, such fundamental and analytical results on this type of sample have never been reported in the literature. The aggregation process of **AdBdy** can be described with only three key spectral components, each of them refering to a specific type of molecular species as discussed below.

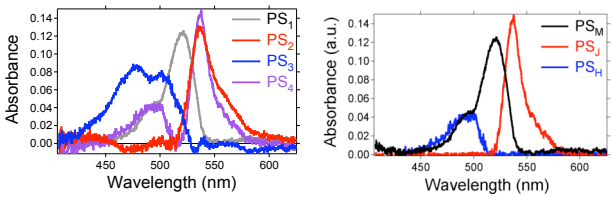

Figure 5. Projection spectra $\{\mathbf{PS_{i=1,2,3,4}}\}$ (left) and $\{\mathbf{PS_{i=M,\ J,\ H}}\}$ (right).

Table 2. Spectroscopic characteristics of the projection spectra $\mathbf{PS_M}$, $\mathbf{PS_J}$ and $\mathbf{PS_H}$.

	$\lambda_{max,abs}$ (nm)	$FWHM_{abs}$ (cm^{-1})
$\mathbf{PS_M}$	521 ± *0,5*	1061 ± *30*

PS_J	537 ± *0,5*	641 ± *30*
PS_H	≈ 494	≈ 1410
S_{PMMA}	517 ± *0,5*	656 ± *38*

The spectroscopic features of the projection spectra (Figure 5 and Table 2) support the presence of three spectroscopically distinguishable components along the aggregation process. According to the exciton theory, **PS_M**, **PS_H**, **PS_J** show similarities with respectively a monomer species in PMMA, an H aggregate and a J aggregate, based on the position of their absorption maximum. Some discrepancies can be pointed out though. While, the 3 nm difference between the absorption maxima of **PS_M** and **AdBdy** in S_{PMMA} can be attributed to the solvatochromic effect (see section Spectroscopic properties in solution), the difference in $FWHM_{abs}$ is much more noticeable as it is twice as much for **PS_M** compared to **AdBdy** in S_{PMMA}. **PS_H** shows a broad absorption band ($FWHM_{abs}$ = 1410 cm^{-1}) as it could be expected for H-aggregates. This feature can also indicate a rather random orientation for these aggregates. Although $FWHM_{abs}$ of **PS_J** has the same order of magnitude as that of S_{PMMA}, it is more than expected for a J aggregate[xx]. This can be explained by either a random orientation of the J aggregates or a small aggregation number. The shape of **PS_J**, unusual for J-aggregates as it rises steeply on the blue side and goes down more gradually on the red side, also suggests that there is not a single type of J-aggregate but a distribution of different packing.

Although the adamantyl substituents do not completely avoid aggregation, they do greatly reduce it as the weight of the monomer component **PS_M** is higher than *ca.* 60% in the concentration range 0.067 – 1.2 M (Figure 6d), which means that non-aggregated molecules exist predominantly in PMMA films. Figure 6d–f clearly show a concentration frontier at 0.29 M (**F6**), which distinguish two different behaviors in the aggregation process. From 0.067 M to 0.29 M, the relative importance of monomer molecules (w_M) decreases to the benefit of H and J aggregate weights (respectively w_H and w_J). Above 0.29 M, w_M seems steady and w_H is on the whole decreasing, within the measurement accuracy, while w_J is still on the increase.

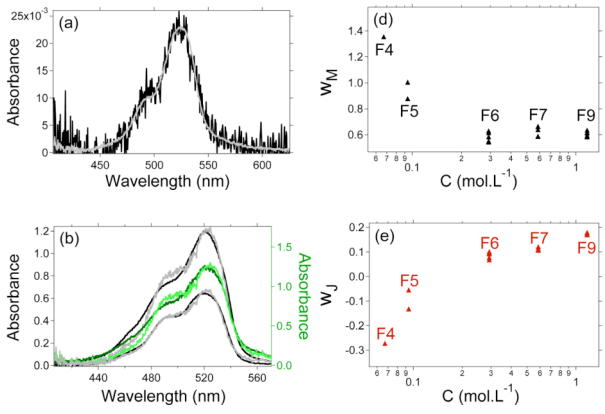

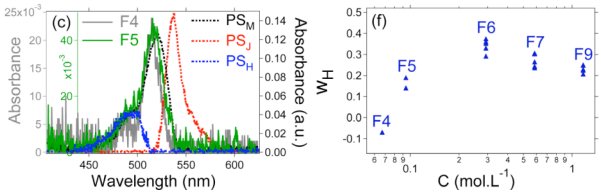

Figure 6. a) An example of a good fitted experimental absorption spectrum (from drop-casted film data). b) Absorption spectra displaying the most important discrepancy in the reconstruction operation: experimental spectrum (line in darker shade) and calculated spectrum based on {**PS_M**, **PS_J**, **PS_H**} (line in brighter shade). c) Absorption spectra of films **F4** (black solid line) and **F5** (green solid line) for which the negative values of w_J and w_H can be explained by a broader absorption band of **PS_M** (black dotted line) and a necessary substraction of **PS_J** (red solid line) and **PS_H** (blue solid line) to **PS_M** to fit the experimental data. d) Weight of **PS_M**, e) **PS_J** and f) **PS_H** versus concentration of **AdBdy** in PMMA films.

Such results strongly remind an equilibrium between the monomer (M) and the J aggregate (J-Agg) containing *n* monomers. Similar observations had been reported for fluorescent amphipathic BODIPY scaffoldings in organogels[xxxvii] and the equilibrium was successfully developed by the Benesi-Hildebrand treatment[xxxviii] according to equations (5) and (6), where K accounts for the equilibrium constant and n_J the aggregation number for the J aggregate. The aggregation number is assumed to be constant.

$$K = [\text{J-Agg}] / [M]^{n_J} \quad (5)$$

$$\ln[\text{J-Agg}] = n_J \ln[M] + \text{constant} \quad (6)$$

The concentrations [J-Agg] and [M] are given by the coefficients c_J and c_M, respectively (see equation 4). Equation (6) can be quite satisfactorily fitted by a linear function with 0.9798 as correlation coefficient (see Figure S14 left in SI). The slope being 1.68 ± 0.06, we can assume that the aggregation number for the J aggregates is 2. This result is of great importance as it proves that **AdBdy** forms preferentially J dimer in condensed phases. The weak aggregation number is coherent with the $FWHM_{abs}$ value, greater than expected for a J-aggregate component (**PS_J**), extracted from the multicomponent analysis.

An attempt has also been made to determine the aggregation number n_H for the H aggregate, using the conservation of matter according to equation (7), where $C_{M,Res}$ corresponds to the concentration of molecules which do not exist as monomers or are involved in J aggregates (see Figure S14 right in SI). The assumption that n_H being constant over the aggregation process is probably at fault. This approach has been unsuccessful.

$$C_{M,Res} = \sum_{i=M,J,H} c_i - c_M - 2c_J = n_H c_H \quad (7)$$

The negative values of w_J (**F4**, **F5**) and w_H (**F4**) can be explained by the obtention routine of the projection spectra, **PS_M** in particular. As a matter of fact, the absorption spectra of **F4** (0.067 M, $FWHM_{abs}$ = 744 ± 27 cm^{-1}) and **F5** (0.094 M, $FWHM_{abs}$ = 901 ± 27 cm^{-1}) are very

similar to the spectrum of **AdBdy** in S_{PMMA} ($FWHM_{abs}$ = 656 ± 38 cm^{-1}, Figure 6c), as the corresponding concentrations are respectively equal and slightly greater than the aggregation concentration limit (0.067 M). Because of the broadness of the absorption band in the calculated $\mathbf{PS_M}$ ($FWHM_{abs}$ = 1061 ± 30 cm^{-1}), the contributions of $\mathbf{PS_J}$ and $\mathbf{PS_H}$ need to be negative in the rebuilt operation (AS_{calc}) in order to fit the experimental date, resulting in negative values for w_J and w_H. As a consequence, the more the concentration approaches the aggregation limit, the more w_J is negative ($|w_J|$ (**F5**) > $|w_J|$ (**F4**)). These artefacts of calculation do not affect the analysis of results as the progressive tendency of each species S_i through the aggregation process is given by the proportional relationship between w_i (respectively c_i) and the weight (respectively concentration) of S_i in the PMMA films. The knowledge of exact weights or concentrations is not necessary in the frame of our objectives.

Although **AdBdy** gives aggregates in condensed phases, the very first statement that the non aggregated molecules being predominant is quite promising concerning the fluorescence efficiency. A relative fluorescent quatum yield was measured for each PMMA film using a methodology which we already reported in previous papers.[xxiii, xxxix] For most PMMA films, several measurements have been done to be assured of the good reliability and reproducibility of the results. The relative quantum yield $\Phi_{Fluo,Rel}$ is assimilated to the ratio $S_{Fluorescence}/I_{488}$ where $S_{Fluorescence}$ is the area of the fluorescence spectrum and I_{488} the absorbed intensity at the excitation wavelength 488 nm. When plotted against the concentration of **AdBdy** in the PMMA films (Figure 7), $\Phi_{Fluo,Rel}$ exhibits the same concentration frontier in the aggregation process and shows a coherent behaviour: from 0.067 M, where the aggregation begins, to 0.29 M, $\Phi_{Fluo,Rel}$ is almost divided by a factor of 5 and is then steady during the equilibrium between the J dimer and the monomer. Relative quantum yields for concentrations below 0.067 M could not be determined because of a too weak absorbance of the films. This result points out a promising optimization of Φ_{Fluo} compared to other dyes in doped polymer films[xxxiv]: for instance, Perylene Red shows a Φ_{Fluo} decreases by a factor of 10 when doped in PMMA at 0.45 M (compared to 1.2 M in our case).[xl]

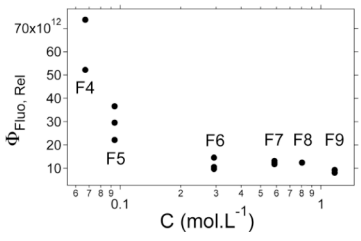

Figure 7. Relative fluorescence quantum yield $\Phi_{Fluo,Rel}$ vs concentration of **AdBdy** in PMMA films.

The first decrease of $\Phi_{Fluo,Rel}$ can be easily explained by the increasing formation of H aggregates, which are known to be non or weakly fluorescent species and efficient traps for excitation energy. As only monomer and H aggregate absorb at 488 nm (Figure 5), the excitation energy is most likely transferred to the emissive J dimers since the fluorescence spectra of films **F6→F9** are different from the monomer emission (Figure 4).

In order to understand the energy transfer mechanism, fluorescence and anisotropy decays have been measured (Figure 8), with an excitation at 515 nm, where absorption is also mainly due to the monomer and H aggregates. The total fluorescence decays I(t) and the anisotropy decays r(t) were calculated using the formulas[xli]:

$$I(t) = I_{\parallel}(t) + 2I_{\perp}(t)$$

$$r(t) = \frac{I_{//}(t) - GI_{\perp}(t)}{I_{//}(t) + 2GI_{\perp}(t)}; G = \frac{I_{//}(t)}{I_{\perp}(t)}$$

where $I_{||}(t)$ (respectively $I_{\perp}(t)$) is the fluorescence decay polarized parallel (respectively perpedicular) to the polarization of the excitation light.

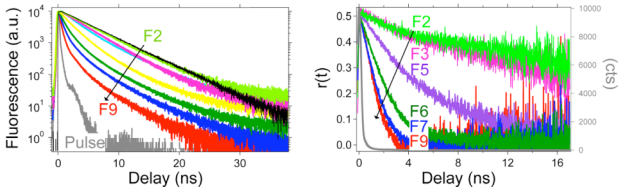

Figure 8. Fluorescence decays (left) and anisotropy decays (right) of **AdBdy** doped in PMMA films, excited at 515 nm. The laser pulse corresponds to the grey curve.

Overall, the fluorescence decays show that the concentration effect gives rise to a growing component with a very short lifetime. This first observation confirms an effective energy transfer from the monomer species to the J dimers, which are also fluorescent. As a matter of fact, on one hand, a high probability of energy transfer between the different species shortens the time that monomer species remain in their excited state. On the other hand, if quenching were due to only non fluorescent aggregates, no change in lifetime would be expected because these aggregates do not contribute to the signal, in a static quenching mechanism. An existing energy transfer between molecules is all the more corroborated by the anisotropy decays which become faster with increased dye concentration. Indeed, when a molecule is excited in a certain polarization direction, it will generally decay with the same polarization in solid state or when immobilized. However, when energy is transferred to acceptors with a different orientation than the donor molecule, the fluorescence becomes depolarized. In our case, the donor is the monomer species, which are mainly excited at 515 nm, and the acceptors are the J dimers. We can note that the maximum of anisotropy at t = 0 is higher than the expected value of 0.4 for a standard, single electronic state with a dipole allowed transition.[xli] This can be explained by a preferential orientation of the dipoles in the PMMA matrix due to the preparation of the sample by spin-coating[xlii] or presence of scattered light.[xliii]

The fluorescence decays **F2→F4** are multiexponential, which is unexpected since only monomer species are supposed to be present in the PMMA films in this

concentration range. Indeed, if only one emitting monomeric species was to be found, a single exponential fit of fluorescence decays would have been possible as observed by Sonada and *al.*[xliv] Besides, the mean fluorescence lifetime[xliii] $\langle\tau\rangle$ (Table 3) is decreasing from 4.57 ns (**F2**) to 3.92 ns (**F4**), which implies a quenching of the fluorescence. It has been reported that almost all dyes dissolved in glassy polymer matrixes exhibit nonexponential fluorescence decays.[xlv] The authors attribute this behaviour to density fluctuations in the matrix, which do not relax on the time scale of the dye excited state. Thus, different dyes experience slightly different local environments leading to a possible solvatochromic effect. As the spectra do not show any evidence for aggregation and since molecular diffusion are too slow to account for the observed photophysical behaviour, it has been also suggested that the observed quenching is due to the excitation energy being captured by a closely spaced « statistical pair » of molecules, which is a non fluorescent trap.[xlvi] A statistical pair is defined as simply any two dye molecules in the random distribution which are closer than a certain critical distance so that when one of them is excited, they interact strongly and quench the excitation. In our case, the critical distance can be approximated by the statistical average distance *d* between molecules of **AdBdy**, calculated to be 23 Å with the following formula:[xlvii]

$$d = 0.554\ n_p^{-1/3} \qquad (8)$$

where n_p the number of molecules per volume unit.

Table 3. Mean fluorescence lifetime $\langle\tau\rangle$ measured on PMMA films doped with AdBdy. The statistical average distance *d* gives an estimation of the intermolecular distance between two closest dyes in PMMA matrix. The weights of monomer species (w_M), J dimers (w_J) and H aggregates (w_H) are given as percentages.

Film	$\langle\tau\rangle$[a] (ns)	*d* (nm)	w_M (%)	w_J (%)	w_H (%)
F2	4.57	2.29	–	–	–
F3	3.93	1.82	–	–	–
F4	3.92	1.62	84[a]	≈ 0	16[b]
F5	2.82	1.44	84[a]	≈ 0	16[b]
F6	2.18	0.99	70 *± 20*	≈ 0	30 *± 10*
F7	1.78	0.78	61 *± 3*	10 *± 2*	29 *± 3*
F9	1.18	0.62	60 *± 2*	17 *± 1*	23 *± 2*
S_{PMMA}	4.7	–	–	–	–

[a] $\langle\tau\rangle = \int_0^\infty t\,I(t)dt / \int_0^\infty I(t)dt$ [b] value determined on only one measurement, hence an unknown accuracy.

Fluorescence decays **F5→F9** could not be well fitted with either single or double exponential curves and seem to contain a broad range of lifetimes. We evaluated the rate of decay with the mean fluorescence lifetime $\langle\tau\rangle$. As expected, it decreases rapidly at higher dye contents, again indicating the appearance of faster decay modes. This can be explained with the weight of the H aggregate (w_H) and the intermolecular distance between the different present species. This last one can not be so easily determined as the exact concentration of each species is not known, neither is the intermolecular distance within each type of aggregate. However it can be roughly estimated by the statistical average distance *d*. For similar composition in the films (**F4** and **F5**), the reduction of $\langle\tau\rangle$ is probably due to a decrease of *d* from 1.62 nm to 1.44 nm. The apparent small change in *d* has actually great impact on the interaction energy as it is inversely proportional to *d* to the power three or six depending on the nature of the interaction. The increase of w_H accounts for the decrease of $\langle\tau\rangle$ from **F5** to **F6** as excitation energy trapping will be more efficient. For similar weight of H aggregates (**F6→F9**), several reasons can explain the shortening of $\langle\tau\rangle$:

- The quenching of fluorescence by H aggregates is more efficient due to the reduction of *d*, as w_M goes down to the benefit of w_H.

- A decrease of $\langle\tau\rangle$ can also implies that the J dimer has a shorter fluorescence lifetime than the monomer species. A more efficient energy transfer from the monomer to the J dimer, as *d* is decreasing, can be another potential contribution to the decrease of $\langle\tau\rangle$.

We attempted to describe the fluorescence decays by two different models. The first one was developed by Gösele[xlviii] and studied experimentally by Zewail et al.[xlix] It takes into account Förster resonant dipole–dipole homotransfer (between monomer species) and heterotransfer (between monomer species and J dimers). The recorded fluorescence decays were fitted with the following equation:

$$I_f(t) = Cst + I_0 \times \exp\left(-\frac{t}{\tau_1} - \sqrt{\frac{t}{\tau_2}}\right)$$

involving the background level *Cst*, the amplitude I_0 and two time-constants τ_1 and τ_2 (see SI for further explanation about this model).

We also tried to fit the decay curves to a model of Klafter and Blumen[l] describing the decay of an excited donor in the presence of acceptors, which are randomly distributed on a fractal of Hausdorff dimension d_H:

$$I_f(t) = I_0 \exp\{-t/\tau_0 - P(t/\tau_0)^{d/s}\} \qquad (9)$$

with s the order of the molecular interaction (s = 6 for the usual Förster dipole–dipole mechanism) and P a fitting constant which should be proportional to the acceptor concentration. For integral dimensions, equation (9) reduces to the familiar results of Förster.[li] Equation (9) is known to work very well, giving usually a value roughly between 1.5 and 3 for d_H.[xli,lii]

None of these quite diverse quenching models describes the data very well. Because they all assume a homogeneous distribution of dye molecules, this could be an indication that the distribution is not homogeneous. We were not able to describe the anisotropy decays by the Gouchanour–Anderson–Fayer theory.[liii] The encountered difficulties in fitting may be due to the absence of wavelength selection

when recording anisotropy and fluorescence decays. The latest do depend upon the wavelength of analysis. The data have been collected on the whole fluorescence band, mostly because of the configuration of our setup. The blue-edge can't be effectively probed as we excite the sample at 515 nm with a dichroic mirror operating in the [450-520] nm range, which overlaps with the blue-edge of the fluorescence band.

Some important conlusions can nevertheless be drawn from the shown data: 1) whereas fluorescence quenching is sensitive to the total distance covered by the excitation energy during its lifetime, anisotropy probes the first transfer event away from the initially excited molecule. One can thus say that this first step of the transfer is all the more fast that the concentration of **AdBdy** in the PMMA is high, which is coherent with a decreased intermolecular distance *d*. 2) as shown on the figure 8, the anisotropy decay times are much shorter compared to the fluorescence decays. For the most concentrated films (F6 to F9), the anisotropy relaxes to zero within 8 ns, which is almost four times faster than the fluorescence decays (35 ns). This result is completely coherent with our previous statement that most of the molecules are still present as monomers in the polymer matrices.

3. Conclusion

A new sterically hindered boron-dipyrromethene (BODIPY) dye has been engineered and synthesized by modification of the pyrrole substituents. Adamantyl moieties have been grafted for the first time on the BODIPY core. This was done to avoid π-π stacking, usually observed with conjugated substituents and leading to a loss of fluorescence quantum yield in condensed phases, On top of being a completely saturated moiety, this substituent has a "ball shape" like geometry, which can be an additional element to keep the molecules apart in condensed phases. The spectroscopic properties in different solvents are presented. Effects of adamantyl groups on aggregation behaviour are studied in poly(methyl methacrylate) (PMMA) films doped with the BODIPY dye (concentration range of 0.47 mM – 1.2 M). Absorption, emission, relative fluorescence quantum yield, fluorescence lifetime and time-resolved anisotropy measurements are carried out. A concentration limit for aggregation is determined to be 0.067 M. An original analysis of multicomponents has been done on the absorption spectra of the BODIPY dye in PMMA and drop-casted films. The results showed that the aggregation process of the adamantyl substituted BODIPY can be quite fairly described by three distinguishable components which correspond to a monomer species, a J dimer and H aggregates. Each component has also been spectroscopically well characterized, which is a significant result considering the fact that the aggregates did not need to be isolated. The aggregation process in the PMMA films clearly shows that from 0.067 M (concentration limit for aggregation) to a concentration frontier at 0.29 M, the monomer species decrease to the benefit of J- and H aggregates. Above 0.29 M the monomer species are steady whereas the J aggregate concentration increases, which has been successfully described by an equilibrium between the monomer species and the J aggregates, giving an aggregation number of two for these latest. The formation of H aggregates is likely to be more complicated over the studied concentration range as attempts to determine their aggregation number were unsuccessful. From 0.067 M to 0.29 M the relative fluorescence quantum yield ($\Phi_{Fluo, Rel}$) is only reduced by one fifth compared to the dye in solution, which supports again the good effectiveness of adamantyl substituents concerning loss of fluorescence due to aggregation. Above the 0.29 M frontier, $\Phi_{Fluo, Rel}$ is steady. Analysis of fluorescence and anisotropy decays shows that the excitation energy is transferred by the monomer species to the J dimer, and very probably trapped by H aggregates as the mean fluorescence lifetime decreases when the BODIPY concentration increases in the PMMA films. However usual theoretical models based on a Förster resonance energy transfer failed to describe the measured decays. Further work will be carried out to elaborate a suitable theoretical model in order to account for the energy transfer mechanism. A spectroscopic study and a computational work on micro-crystals and amorphous nano-particles of **AdBdy** are in process in order to determine physical constants such as the intermolecular coupling energy and insights on the mechanism of the exciton delocalization within the organized solid state. With such a high concentration limit for aggregation (0.067 $mol.L^{-1}$) and an efficiently preserved fluorescence quantum yield (Φ_{Fluo} divided by only 5 for highly doped films), **AdBdy** could offer great interest for hybrid organic-inorganic materials such as stable organic nano-particles (crystalline or amorphous) grown in sol–gel thin films,. Another possibility is to incorporate nano-particles of **AdBdy** into polymer matrices. In that perspective, elaboration of size-controlled nano-particles of **AdBdy** by a microfluidic process is currently carried out in our group.

4. EXPERIMENTAL SECTION

4.1. Sample preparation

^{1}H, ^{13}C, ^{19}F and ^{11}B NMR spectra were recorded in $CDCl_3$ on a JEOL ECS (400 MHz) spectrometer. All chemical shifts are referenced to Me_4Si (TMS). Coupling constants (J) values are given in Hz.

Drop-casted films (amorphous deposits) were prepared by quick evaporation of a droplet of the dye in solution (about 10^{-5} to 10^{-6} M) in dichloromethane onto microscope slides.

Poly(methyl methacrylate) (PMMA, m_{PMMA} = 45.4 mg, 120 000 average molecular weight, density d_{PMMA} = 1.188) was dissolved in toluene ($V_{toluene}$ = 5 mL, $d_{toluene}$ = 0.8669). The solution was stirred over night. In order to prepare films of PMMA doped with a wide range of different concentrations of dye, solutions of **AdBdy** were previously prepared in dichloromethane (concentration $c_{dye, DCM}$ $mol.L^{-1}$). The dye solution (V_{dye} = 700 or 500 µL) was then mixed with PMMA solution in toluene (V_{PMMA} = 200 µL) for 3 hours under ultrasonic stirring.

Dichloromethane was then removed under vacuum at 60°C. The final concentration of PMMA in toluene is 1% w/w. The films of PMMA were prepared by standard spin-coating technique. Glass microscope slides (cut to 22 mm × 22 mm) were washed with ethanol, wiped clean and placed on a spin coater. While the glass slide was spinning at 3000 rpm, 40 µL of the dye/PMMA mixture in toluene was added using a pipette. The spin coating was stopped after 60 seconds. The final concentrations of **AdBdy** in the PMMA films ($C^{mol/g_{PMMA}}_{dye,PMMA}$ moles dye g^{-1} of PMMA; $C^{mol/L}_{dye,PMMA}$ moles dye L^{-1}) were determined using the formulas:

$$C^{mol/g_{PMMA}}_{dye,PMMA} = \frac{c_{dye,DCM} \times V_{dye} \times V_{toluene} \times 10^{-3}}{V_{PMMA} \times \left(V_{toluene} d_{toluene} + m_{PMMA} \times 10^{-3}\right)} \times \frac{m_{PMMA} + V_{toluene} d_{toluene}}{m_{PMMA}}$$

$$C^{mol/L}_{dye,PMMA} = \frac{C^{mol/g_{PMMA}}_{dye,PMMA} \times d_{PMMA} \times 10^{3}}{1 + V_{dye} N_A \times C^{mol/g_{PMMA}}_{dye,PMMA} \times d_{PMMA} \times 10^{3}}$$

In the above formulas, the volumes and weights are expressed in mL and mg, respectively. N_A is the Avogadro's constant. The $C^{mol/L}_{dye,PMMA}$ notation correspond to the C notation in the text.

Blank samples of PMMA were synthesized and processed in the same manner as the dye-doped samples. They were used as reference samples.

4.2. Procedure for the synthesis of AdBdy

Pyrrole[xxiv] (0.237 g, 1.18 mmol) and 2,4,6-trimethylbenzaldehyde (0.097 g, 0.59 mmol) were dissolved in 25mL of degassed CH_2Cl_2, then 2-4 drops of trifluoroacetic acid (TFA) were added, and the obtained solution was stirred under argon at room temperature for 4 hrs. Then 0.134 g (0.59 mmol) of 2,3-dichloro-5,6-dicyano-*p*-benzoquinone (DDQ) was added and the reaction mixture was stirred for 0.5 h. After that, diisopropylethylamine (0.72 ml, 4.13 mmol) and boron trifluoride etherate (0.82 ml, 6.49 mmol) were added with subsequent stirring of the obtained dark colored solution for 0.5 h. After evaporation of the solvent at ambient temperature in vacuo the residue was chromatographed on silica (CH_2Cl_2–petroleum ether = 1/3 v/v) to afford 0.239 g (70% yield) of BODIPY. ^{1}H NMR ($CDCl_3$, 400 MHz): δ = 6.92 (s, 2H, $H_{mesityl}$), 6.48 (d, 2H, $^3J_{H-H}$ = 4.1 Hz, $H_{pyrrole}$), 6.41 (d, 2H, $^3J_{H-H}$ = 4.12 Hz, $H_{pyrrole}$), 2.35 (s, 3H, $CH_{3mesityl}$), 2.27 (bs, 12H, $CH_{2adamantyl}$), 2.13 (m, 6H, $CH_{adamantyl}$), 2.09 (s, 6H, $CH_{3mesityl}$), 1.81 (m, 12H, $CH_{2adamantyl}$) ppm. ^{13}C NMR ($CDCl_3$, 100 MHz): δ = 171.1, 142.9, 138.2, 137.0, 136.4, 131.1, 129.0, 128.0, 117.5, 41.1, 37.5, 36.8, 28.9, 21.2, 20.2 ppm. ^{11}B NMR ($CDCl_3$, 128 MHz): δ = 0.61 (t, $^2J_{B-F}$ = 34.5 Hz) ppm. HR-MS (ESI): *m/z* [M + Na]$^+$ calculated for $C_{38}H_{45}N_2F_2{}^{11}BNa^+$ = 601.3542, found 601.3531.

4.3. Steady-state and time resolved spectroscopy in solution

Solvents used were all of spectroscopic grade. They were purchased from Sigma-Aldrich. U.V.–visible spectra were recorded on a Varian Cary (Palo Alto, CA USA) double beam spectrometer using a 10mm path quartz cell from Thuet (Bodelsheim, France). Excitation and emission spectra were measured on a SPEX Fluoromax-3 (Horiba Jobin-Yvon). A right-angle configuration was used. The solvents were spectrometric grade. For liquid samples, optical density was adjusted below 0.1 to avoid reabsorption artifacts.

The fluorescence decay curves were obtained with a time-correlated single-photon-counting method using a titanium-sapphire laser (82 MHz, repetition rate lowered to 4MHz thanks to a pulsepeaker, 1 ps pulse width, a doubling crystals is used to reach 495 nm excitation) pumped by an argon ion laser from Spectra Physics (Mountain View, CA, USA). The detection polarizer was set to the magic angle 54.7° with respect to the incident beam to negate the effects of rotational diffusion.[xli] The Levenberg-Marquardt algorithm was used for non-linear least square fit as implemented in the Globals software (Globals Unlimited, Villa Grove, USA). The quality of the fit was estimated by the residuals, i.e. the difference between the measured value and the fit, divided by the square root of the fit. χ^2 is equal to the variance of the weighted residuals. A fit was said appropriate for χ^2 values between 0.8 and 1.2.

4.4. Steady-state and time resolved spectroscopy in films

Photophysical properties of drop-casted films and PMMA films doped with **AdBdy** were studied on an inverted Nikon TE2000 microscope using a × 60, × 40 or × 10 objective (0.95, 0.75 and 0.5 numerical apertures for × 60, × 40 and × 10 objectives, respectively). The fluorescence excitation at 515 nm was provided by a T-Pulse 200 Amplitude laser (1030 nm, 10.1 MHz, 407 fs pulse width, a doubling crystalsis used to reach 515 nm excitation). The fluorescence excitation at 488 nm was provided by a argon ion laser from Optilas (Ion Laser Technology). The fluorescence excitation at 470 nm was provided by a photodiode from Thorlabs (LEDC6 Mounted & Collimated LED). The sample was irradiated using a wide field configuration. For each selected position on a film, the transmission and fluorescence pictures of the region were taken with a Nikon camera, and the absorption and emission spectra (34, 79 and 1.3 × 10^3 µm^2 area for × 60, × 40 and × 10 objectives, respectively) were recorded using a fiber spectrophotometer (Ocean Optics, Inc.). Thanks to the measurements obtained at different positions on cast films, we could plot the surface of each emission spectrum as a function of the corresponding absorbance at 488 or 470 nm and estimate a relative fluorescence quantum yield.

The fluorescence spectra, recorded with the Ocean Optics fiber spectrophotometer, were corrected of the inner filter effect following the formula:

$$I_f(\lambda) = \left(\frac{A(\lambda_{exc}) + A(\lambda)}{A(\lambda_{exc})}\right)\left(\frac{1 - 10^{-A(\lambda_{exc})}}{1 - 10^{-A(\lambda_{exc}) - A(\lambda)}}\right) I_{f,\exp}(\lambda) \qquad (10)$$

where $I_f(\lambda)$ is the corrected spectrum, $I_{f,\ exp}(\lambda)$ the recorded spectrum, $A(\lambda)$ the absorption spectrum and $A(\lambda_{exc})$ the absorbance of the sample at the excitation wavelength. The fluorescence spectra were also corrected of the detector sensibility.

Time-resolved fluorescence experiments on films were performed using a space and time correlated photon-

counting photomultiplier (QA) from Europhoton Gmbh (Berlin) mounted onto the microscope. This detector enables us to perform scanning-less fluorescence imaging by recording both intensity images and FLIM. The whole setup has been described previously.[liv] Briefly, the QA consists in a multichannel plate photomultiplier working in the single photon counting mode. The anode is divided into four quadrants. A fifth conductive part is placed around these four anodes in order to improve the detector precision for points located at the borders of the field. When a photoelectron is produced, an avalanche is created in the two multichannel plates and spread over the five anodes. The position of the photon on the photocathode can be calculated from a weighted mean of the five charges collected. For each photon detected, the delay between the laser pulse and the arrival of the photon on the PM, the absolute arrival time (i.e., the time from the beginning of the measurement) and the position of the photon on the photocathode are measured and saved on a hard disk. The histogram of the number of photon collected per pixel gives an intensity image of the sample. The histogram of the number of photons collected as a function of absolute arrival time gives the evolution of the global fluorescence intensity and a way to monitor photobleaching. The average fluorescence lifetime τ for each pixel was calculated by dividing the sum of all the delays τ_i by the number of photons N arrived on that pixel, i.e., $\tau = (1/N)\sum_1^N \tau_i$. It is a fast and robust way to do FLIM. Fluorescence decays were built as the histogram of the number of photon collected as a function of the fluorescence delay. The collection is done over all the pixels in a specific area. Unless otherwise stated, the fluorescence lifetimes given in this paper correspond to the global fluorescence decay, i.e. the decay corresponding to the whole QA image. The instrument response time is 150 ps (fwhm) and the spatial resolution of our setup is 300 nm (fwhm). The quality of the fit was estimated by the weighted residuals. χ^2 is equal to the variance of the weighted residuals. A fit was said appropriate for χ^2 values between 0.8 and 1.2.

4.5. Quantum Chemical Calculations

Calculations were performed with the Gaussian software (Gaussian 03, Revision C.02)51 at the MESO calculation center of the ENS Cachan (NecTX7 with 32 processors Itanium 2). All calculations were performed using the B3LYP/6-31+G(d) method.

4.6. X-ray diffraction

The **AdBdy** crystal structure determination was first carried out using single crystal X-ray diffraction. Thus, IP-BDPY single crystal, obtained by slow evaporation of CH_2Cl_2 solution, was mounted on a Rigaku rotating-anode diffractometer, equipped with a MM007 HF generator, delivering filtered Cu-Kα radiation (λ = 1.54187 Å) enhanced and collimated by Osmic confocal optics and with a Rapid II Curved Image Plate. Crystal data of $C_{38}H_{45}BF_2N_2$ recorded at 200 K: Mr = 578.57 g.mol^{-1}, orange-red prismatic crystal (0.42 × 0.36 × 0.28 mm), Monoclinic space group, P $2_1/c$ (n°14), a = 14.0557 (3) Å, b = 11.4779(3) Å, c = 19.3737(13) Å, β= 98.905(7)°, and V = 3087.9(2) Å^3, Z = 4, ρ_{calcd} = 1.245 g.cm^{-3}, μ = 0.626 mm^{-1}. 20448 measured reflections ($2\theta_{max}$ = 144.2°) and 5770 independent reflections with R_{int} = 0.0586. The reflections were corrected for Lorentz and polarization effects as well as for absorption using a multi-scan approach. The structure was solved by direct methods with SHELX97-S program[lv] and refined by full matrix least-squares, based on F^2, using the SHELX97-L software[lv] through the CRYSTALBUILDER interface.[lvi] All non-hydrogen atoms were refined with anisotropic thermal parameters. Hydrogen atoms were generated in idealized positions, riding on the carrier atoms, with isotropic thermal parameters. The final cycle refinement including 392 parameters converged to R1 = 0.0491 (4393 data with I > 2σ(I)) and wR2 = 0.1488 (all 5756 data), Goodness of Fit S=1.152, max./min. residual electron density 0.238/-0.205. ORTEP[lvii] drawing and packing studies were carried out using MERCURY.S[lviii] See supporting CIF file for further refinement details. CCDC reference number 852756.

CORRESPONDING AUTHOR

Rachelm@ppsm.ens-cachan.fr; Thanh.vu@ppsm.ens-cachan.fr

REFERENCES

[i] (a) Ye, S.; Chen, J.; Di, C.; Liu, Y.; Lu, K.; Wu, W.; Du, C.; Liu, Y.; Shuai, Z.; Yu, G. *J. Mater. Chem.* **2010**, *20*, 3186–3194; (b) Liu, Y.; Tao, X.; Wang, F.; Dang, X.; Zou, D.; Ren, Y.; Jiang, M. *Org. Electron.* **2009**, *10*, 1082–1090.

[ii] (a) Fan, R.; Xia, Y.; Chen, D. *Opt. Express* **2008**, *16*, 9804; (b) Fukuda, M.; Kodama, K.; Yamamoto, H.; Mito, K. *Dyes Pigm.* **2004**, *63*, 115–125.

[iii] (a) Costela, A.; García-Moreno, I.; Sastre, R.; Materials for solid state dye lasers. In Handbook of Advanced Electronic and Photonic Materials, Vol. 7 (Edited by H. S. Nalwa), **2001**, pp. 161–208. Academic Press, New York. [Chap. 4]. (b) Chénais, S.; Forget, S. *Polymer International* **2012**, *61*, 390–406.

[iv] (a) Park, S.-Y.; Kubota, Y.; Funabiki, K.; Shiro, M.; Matsui, M. *Tetrahedron Lett.* **2009**, *50*, 1131–1135; (b) Park, S.-Y.; Ebihara, M.; Kubota, Y.; Funabiki, K.; Matsui, M. *Dyes Pigm.* **2009**, *82*, 258–267.

[v] (a) Kubota, Y.; Uehara, J.; Funabiki, K.; Ebihara, M.; Matsui, M. *Tetrahedron Lett.* **2010**, *51*, 6195-6198. (b) Gao, F.; Liao, Q.; Xu, Z.-Z.; Yue, Y.-H.; Wang, Q.; Zhang, H.-L.; Fu, H.-B. *Angew. Chem., Int. Ed.* **2010**, *49*, 732–735; (c) Imai, Y.; Kamon, K.; Tajima, N.; Kinuta, T.; Sato, T.; Kuroda, R.; Matsubara, Y. *J. Lumin.* **2010**, *130*, 954–958 (d) Shiota, N.; Kinuta, T.; Sato, T.; Tajima, N.; Kuroda, R.; Matsubara, Y.; Imai, Y. *Cryst. Growth Des.* **2010**, *10*, 1341–1345.

[vi] Gómez-Durán, C. F. A.; García-Moreno, I.; Costela, A.; Martin, V.; Sastre, R.; Bañuelos, J.; Arbeloa, F. L.; Arbeloa, I. L.; Peña-Cabrera, E. *Chem. Commun.* **2010**, 5103–5105.

[vii] (a) Umezawa, K.; Nakamura, Y.; Makino, H.; Citterio, D.; Suzuki, K. *J. Am. Chem. Soc.* **2008**, *130*, 1550–1551; (b) Umezawa, K.; Matsui, A.; Nakamura, Y.; Citterio, D.; Suzuki, K. *Chem. Eur. J.* **2009**, *15*, 1096–1106. (c) Nagai, A.; Chujo, Y. *Macromolecules* **2010**, *43*, 193–200.

[viii] (a) Loudet, A.; Burgess, K. *Chem. Rev.* **2007**, *107*, 4891–4932 (b) Wood, T. E.; Thompson, A. *Chem. Rev.* **2007**, *107*, 1831–1861.

[ix] (a) Bura, T.; Leclerc, N.; Fall, S.; Lévêque, P.; Heiser, T.; Ziessel, R. *Org. Lett.* **2011**, *13*, 6030–6033. (b) Niu, S.; Ulrich, G.;

Retailleau, P.; Ziessel, R. *Org. Lett.* **2011**, *13*, 4996–4999. (c) Li, L.; Han, J.; Nguyen, B.; Burgess, K. *J. Org. Chem.* **2008**, *73*, 1963–1970. (d) Rohand, T.; Qin,W.; Boens, N.; Dehaen,W. *Eur. J. Org. Chem.* **2006**, *2006*, 4658–4663.

[x] (a) Karolin, J.; Johansson, L. B.-A.; Strandberg, L.; Ny, T. *J. Am. Chem. Soc.* **1994**, *116*, 7801–7806. (b) Haugland, R. P. Handbook of Fluorescent Probes and Research Chemicals, 6th ed.; Molecular Probes: Eugene, OR, **1996**. (c) Tan, K.; Jaquinod, L.; Paolesse, R.; Nardis, S.; Di Natale, C.; Di Carlo, A.; Prodi, L.; Montalti, M.; Zaccheroni, N.; Smith, K. M. *Tetrahedron* **2004**, *60*, 1099–1106. (d) Yee, M.-c.; Fas, S. C.; Stohlmeyer, M. M.; Wandless, T. J.; Cimprich, K. A. *J. Biol. Chem.* **2005**, *280*, 29053–29059. (e) Wagner, R. W.; Lindsey, J. S. *Pure Appl. Chem.* **1996**, *68*, 1373–1380.

[xi] Metzker, M. L. WO Patent WO/2003/066812, **2003**.

[xii] (a) Golovkova, T. A.; Kozlov, D. V.; Neckers, D. C. *J. Org. Chem.* **2005**, *70*, 5545–5549. (b) Trieflinger, C.; Rurack, K.; Daub, J. *Angew. Chem., Int. Ed.* **2005**, *44*, 2288–2291.

[xiii] There are many examples and an extensive list of references can be found in ref 19a

[xiv] recent examples (a) Álvarez, M.; Costela, A.; García-Moreno, I.; Amat-Guerri, F.; Liras, M.; Sastre, R.; López Arbeloa, F.; Bañuelos Prieto, J.; López Arbeloa, I. *Photochem. Photobiol. Sci.* **2008**, *7*, 802–813. (b) Costela, A.; García-Moreno, I.; Pintado-Sierra, M.; Amat-Guerri, F.; Liras, M.; Sastre, R.; Arbeloa, F. L.; Prieto, J. B.; Arbeloa, I. L. *J. Photochem. Photobiol. A–Chem.* **2008**, *198*, 192–199. (c) García-Moreno, I.; Amat-Guerri, F.; Liras, M.; Costela, A.; Infantes, L.; Sastre, R.; López Arbeloa, F.; Bañuelos Prieto, J.; López Arbeloa, Í. *Adv. Funct. Mater.* **2007**, *17*, 3088–3098.

[xv] Rousseau, T.; Cravino, A.; Bura, T; Ulrich, G.; Ziessel, R.; Roncali, J. *Chem. Commun.* **2009**, 1673–1675.

[xvi] (a) Zhang, D.; Wen, Y.; Xiao, Y.; Yu, G.; Liu, Y.; Qian, X. *Chem. Commun.* **2008**, 4777–4779 (b) Hepp, A.; Ulrich, G.; Schmechel, R.; Von Seggern, H.; Ziessel, R. *Synth. Met.* **2004**, *146*, 11–15.

[xvii] (a) Birks, J. B. In *Photophysics of Aromatic Moelcules*; Wiley: London, **1970**. (b) Auweter, H.; Haberkorn, H.; Heckmann, W.; Horn, D.; Lüddecke, E.; Rieger, J.; Weiss, H. *Angew. Chem., Int. Ed.* **1999**, *38*, 2188–2191.

[xviii] (a) McRae, E. G.; Kasha, M. *Physical Process in Radiation Biology*; Academy Press: New York, **1964**. (b) Ozdemir, T.; Atilgan, S.; Kutuk, I.; Yildirim, L. T.; Tulek, A.; Bayindir, M.; Akkaya, E. U. *Org. Lett.* **2009**, *11*, 2105–2107. (c) Kasha, M.; Rawls, H. R.; El-Bayoumi, M. A. *Pure Appl. Chem.* **1965**, *11*, 371–392.

[xix] Birks, J. B. In Photophysics of Aromatic Molecules; Wiley: London, **1970**.

[xx] Würthner, F.; Kaiser, T. E.; Saha-Möller, C. R. *Angew. Chem. Int. Ed.* **2011**, *50*, 3376–3410.

[xxi] Martínez Martínez, V.; López Arbeloa, F.; Bañuelos Prieto, J.; Arbeloa López, T.; López Arbeloa, I. *J. Phys. Chem. B* **2004**, *108*, 20030–20037.

[xxii] (a) Méallet-Renault, R.; Herault, A.; Vachon, J. J.; Pansu, R. B.; Amigoni-Gerbier, S.; Larpent, C. *Photochem. Photobiol. Sci.* **2006**, *5*, 300–310. (b) Zaitsev, A. B.; Méallet-Renault, R.; Schmidt, E. Y.; Mikhaleva, A. I.; Badre, S.; Dumas, U.; Vasil'tsov, A. M.; Zorina, N. V.; Pansu, R. B. *Tetrahedron* **2005**, *61*, 2683–2688. (c) Badré, S.; Monnier, V.; Méallet-Renault, R.; Dumas-Verdes, C.; Schmidt, E. Y.; Mikhaleva, A. I.; Laurent, G.; Levi, G.; Ibanez, A.; Trofimov, B. A.; Pansu, R. B. *J. Photochem. Photobiol. A* **2006**, *183*, 238–246.

[xxiii] Vu, T. T.; Badré, S.; Dumas-Verdes, C.; Vachon, J.-J.; Julien, C.; Audebert, P.; Senotrusova, E. Y.; Schmidt, E. Y.; Trofimov, B. A.; Pansu, R. B.; Clavier, G.; Méallet-Renault, R. *J. Phys. Chem. C* **2009**, *113*, 11844–11855.

[xxiv] Trofimov, B. A.; Schmidt, E. Y.; Zorina, N. V.; Senotrusova, E. Y.; Protsuk, N. I.; Ushakov, I. A.; Mikhaleva, A. b. I.; Méallet-Renault, R.; Clavier, G. *Tetrahedron Lett.* **2008**, *49*, 4362–4365.

[xxv] (a) Garcia, O.; Sastre, R.; delAgua, D.; Costela, A.; Garcia-Moreno, I.; Lopez Arbeloa, F.; Banuelos Prieto, J.; Lopez Arbeloa, J. *J. Phys. Chem. C* **2007**, *111*, 1508-1516. (b) García, O.; Sastre, R.; del Agua, D.; Costela, A.; García-Moreno, I. *Chem. Mater.* **2006**, *18*, 601-602.

[xxvi] Botzung-Appert, E.; Monnier, V.; Duong, T. H.; Pansu, R.; Ibanez, A. *Chem. Mater.* **2004**, *16*, 1609-1611.

[xxvii] Calvo-Muñoz, M. L.; Truong, T. T.; Tran-Thi, T. H. *Sens. Actuators, B* **2002**, 87, 173.

[xxviii] (a) Chen, J.; Burghart, A.; Derecskei-Kovacs, A.; Burgess, K. *J. Org. Chem.* **2000**, *65*, 2900–2906. (b) Kee, H. L.; Kirmaier, C.; Yu, L.; Thamyongkit, P.; Youngblood, W. J.; Calder, M. E.; Ramos, L.; Noll, B. C.; Bocian, D. F.; Scheidt, W. R.; Birge, R. R.; Lindsey, J. S.; Holten, D. *J. Phys. Chem B* **2005**, *109*, 20433–20443. (c) Mula, S.; Ray, A. K.; Banerjee, M.; Chaudhuri, T.; Dasgupta, K.; Chattopadhyay, S. *J. Org. Chem.* **2008**, *73*, 2146–2154.

[xxix] (a) Bandichhor, R.; Thivierge, C.; Bhuvanesh, N. S. P.; Burgess, K. *Acta. Crystallogr., Sect. E* **2006**, *62*, o4310–o4311. (b) Wang, D. C.; Wang, H. P.; Gao, S.; Zhang, T. Y.; Peng, X. J. *Acta. Crystallogr., Sect. E* **2007**, *63*, o2238–o2239.

[xxx] Qin, W.; Baruah, M.; Sliwa, M.; Van der Auweraer, M.; De Borggraeve, W. M.; Beljonne, D.; Van Averbeke, B.; Boens, N. *J. Phys. Chem. A* **2008**, *112*, 6104–6114.

[xxxi] Catalán, J. *J. Phys. Chem. B* **2009**, *113*, 5951–5960.

[xxxii] Qin, W.; Baruah, M.; Sliwa, M.; Van der Auweraer, M.; De Borggraeve, W. M.; Beljonne, D.; Van Averbeke, B.; Boens, N. *J. Phys. Chem. A* **2008**, *112*, 6104–6114.

[xxxiii] Bojarski, P.; Kaminska, A.; Kulak, L.; Sadownik, M. *Chem. Phys. Lett.* **2003**, *375*, 547–552.

[xxxiv] Imhof, A.; Megens, M.; Engelberts, J. J.; de Lang, D. T. N.; Sprik, R.; Vos, W. L. *J. Phys. Chem. B* **1999**, *103*, 1408–1415.

[xxxv] Kubista, M.; Sjöback, R.; Nygren, J. *Anal. Chim. Acta* **1995**, *302*, 121–125.

[xxxvi] Abdi, H.; Williams, L. J.; Wiley *Interdisciplinary Reviews: Computational Statistics* **2010**, *2*, 433-459.

[xxxvii] Camerel, F.; Bonardi, L.; Ulrich, G.; Charbonnière, L.; Donnio, B.; Bourgogne, C.; Guillon, D.; Retailleau, P.; Ziessel, R. *Chem. Mater.* **2006**, *18*, 5009–5021.

[xxxviii] Benesi, H.; Hildebrand, J. H. *J. Am. Chem. Soc.* **1949**, *71*, 2703–2707.

[xxxix] Schmidt, E. Y.; Trofimov, B. A.; Mikhaleva, A. b. I.; Zorina, N. V.; Protzuk, N. I.; Petrushenko, K. B.; Ushakov, I. A.; Dvorko, M. Y.; Méallet-Renault, R.; Clavier, G.; Vu, T. T.; Tran, H. T. T.; Pansu, R. B. *Chem. Eur. J.* **2009**, *15*, 5823–5830.

[xl] Fennel, F.; Lochbrunner, S. *Phys. Chem. Chem. Phys.* **2011**, *13*, 3527–3533.

[xli] Valeur, B. *Molecular Fluorescence. Principles and Applications*; Wiley-VCH: Weinheim, **2002**.

[xlii] Lakowicz, J. R.; Gryczynski, I.; Gryczynski, Z.; Dattelbaum, J. D. *Anal. Biochem.* **1999**, *267*, 397–405.

[xliii] Lakowicz, J. R. *Principles of fluorescence spectroscopy*, 3rd ed.; Springer: New York, **2007**.

[xliv] Sonoda, Y.; Goto, M.; Tsuzuki, S.; Tamaoki, N. *J. Phys. Chem. A* **2006**, *110*, 13379–13387.

[xlv] Yang, J.; Roller, R. S.; Winnik, M. A. *J. Phys. Chem. B* **2006**, *110*, 11739–11745.

[xlvi] Boulu, L. G.; Patterson, L. K.; Chauvet, J. P.; Kozak, J. J. *J. Chem. Phys.* **1987**, *86*, 503–507.

[xlvii] Berberan-Santos, M. *Am. J. Phys.* **1986**, *54*, 1139–1141.

[xlviii] (a) Gösele, U.; Hauser, M.; Klein, U. K. A.; Frey, R. *Chem. Phys. Lett.* **1975**, *34*, 519–522. (b) Klein, U. K. A.; Frey, R.; Hauser, M.; Gösele, U. *Chem. Phys. Lett.* **1976**, *41*, 139–142.

[xlix] Millar, D. P.; Robbins, R. J.; Zewail, A. H. *J. Chem. Phys.* **1981**, *75*, 3649–3659.

[l] (a) Klafter, J.; Blumen, A. *J. Chem. Phys.* **1984**, *80*, 875–877. (b) Levitz, P.; Drake, J. M.; Klafter, J. *J. Chem. Phys.* **1988**, *89*, 5224–5236.

[li] (a) Förster, n. *Th. Z. Naturforsch.* **1949**, *4a*, 321. (b) Förster, T. *Ann. Phys. (Leipz)* **1948**, *2*, 55.

[lii] Nakashima, K.; Duhamel, J.; Winnik, M. A. *J. Phys. Chem.* **1993**, *97*, 10702–10707.

[liii] Baumann, J.; Fayer, M. D. *J. Chem. Phys.* **1986**, *85*, 4087–4107.

[liv] Spitz, J. A.; Yasukuni, R.; Sandeau, N.; Takano, M.; Vachon, J. J.; Meallet-Renault, R.; Pansu, R. B. *J. Microsc.* **2008**, *229*, 104–114.

[lv] Sheldrick, G.M. *Acta Cryst.* **2008**, **A**64, 112–122.

[lvi] Welter, R. *Acta Cryst.* **2006**, **A**62, s252.

[lvii] Burnett, M. N.; Johnson, C K. *Oak Ridge National Laboratory Report ORNL-6895*, **1996**.

[lviii] Macrae, C. F., Edgington, P. R., McCabe, P., Pidcock, E., Shields, G. P., Taylor, R., Towler, M. & van de Streek, J. *J. Appl. Cryst.* **2006**, 39, 453–457.

TABLE OF CONTENTS GRAPHIC